Lightweight Heat Pipe Cooling Solution for High-Frequency Transformer in Power Electronics Building Block

David E. Hernandez

MIT Sea Grant Design Laboratory Department of Mechanical Engineering Massachusetts Institute of Technology Cambridge, MA 02139 USA email: davidh04@alum.mit.edu

Julie S. Chalfant¹

MIT Sea Grant Design Laboratory Department of Mechanical Engineering Massachusetts Institute of Technology Cambridge, MA 02139 USA email: chalfant@mit.edu Power Electronics Building Blocks provide a modular method of accomplishing power conversion for naval vessels; a key challenge in the development of PEBBs is thermal management. This study explores the feasibility of using heat pipes in conjunction with a chilled cold plate to maintain PEBB transformer core and coil temperatures below 100°C and 155°C respectively. First, a standalone thermal model of the transformer was built in StarCCM+ and used to test various cooling solutions. The proposed design uses 16 copper-water heat pipes configured to provide alternative paths of heat flow for the regions of the transformer furthest from the cold plate. Shapal HiM Soft Machinable AlN ceramic provides high voltage insulation. Electromagnetic simulations estimated the induced losses in the heat pipes as a result of high-frequency coil operations. The final configuration achieved a core maximum temperature of 99.7°C, coil maximum of 93.2°C, and MOSFET maximum of 144.6°C, all within their respective limits despite the induced losses in the copper-walled heat pipes. The usage of heat pipes adds only 0.29 kg to the weight-constrained PEBB. The thermal results showcase the effectiveness of heat pipes in the PEBB and invite further analysis and experimentation to validate the electromagnetic implications of the concept. These results also contribute to the general ongoing study of heat pipe usage near high-frequency electronics.

Keywords: heat pipes, high-frequency transformer, indirect liquid cooling

Introduction

The demand for improved performance and enhanced capabilities onboard naval vessels has increased the complexity of the electrical systems required to meet these goals. As a result, areas such as power conversion and distribution are being redesigned in order to modernize operations and prepare for the demands of future technology. One new concept is the Power and Energy Corridor, which aims to meet increased power demands while also grouping the primary electrical distribution and conversion equipment into a compact and modular physical footprint [1]. Modularity of power systems is enhanced through Power Electronics Building Blocks (PEBBs), which are designed to be self-contained and replaceable power conversion units [2]. A PEBB-based power distribution system uses multiple PEBBs in any given subsection, connecting them in series and parallel to deliver the required voltage and current levels, respectively. Such flexibility allows a PEBB-based system to easily scale with the power demands of different ship classes, as well as streamlining the manufacturing and integration processes of future mission requirements. The PEBB is designed to be lightweight and to operate in a "plug-and-play" approach, allowing quick replacement for repairs and maintenance.

In order to meet the power conversion and density requirements, the PEBB must be adequately cooled to ensure the full performance of its internal components. The PEBB is still under development; however, the currently available design sees dominant heat generation through 96 MOSFET switches and a 400kHz transformer, which, under worst case conditions, generate roughly 9.6 kW and 624 W of waste heat respectively [2,3]. The task of thermal management is made more difficult when considering the design limitations specific to the PEBB. The

requirement of being easy to carry limits the weight of a unit to 16 kg and similarly affects its total volume [4]. Furthermore, the desire for a quick attachment and detachment process prohibits the presence of fluid within the PEBB due to the complexities associated with drainage, eliminating the possibility of directly liquid-cooling the internal components.

With this design challenge in mind, a concept that is currently being investigated is that of indirect liquid cooling through a rack-mounted cold plate. The approach would rely on forced convection via the passing fluid to create a chilled heat sink that would be in contact with both the top and bottom outer surfaces of the PEBB. Having the primary cooling hardware detached from the PEBB unit itself addresses both the size and ease-of-removal limitations. Preliminary thermal analysis of this solution on an PEBB model found that the cold plate was effective at lowering component temperatures, but also concluded that the transformer, although lower in total heat output, experiences hot spots exceeding specifications in core regions furthest from the cold plates [5] and in the coils that do not connect directly to the cold plates. For indirect liquid cooling to become a feasible solution, additional hardware must be incorporated to maintain temperatures in these harder-to-reach regions of the transformer.

The scope of this study is to explore the usage of copper-walled heat pipes in conjunction with indirect liquid cooling to provide an acceptable thermal management solution for the PEBB transformer. The development of both the thermal model as well as a preliminary electromagnetic model were completed in Siemens StarCCM+. Proposed solutions were analyzed based on their ability to regulate transformer temperatures, with additional consideration towards potential electromagnetic impacts associated with the high-frequency, medium-voltage operations of the transformer. The goal was to provide a detailed overview of the heat pipe configuration required to pull heat from the transformer core and coil to the common substrate, which will in turn be cooled

¹Corresponding Author.

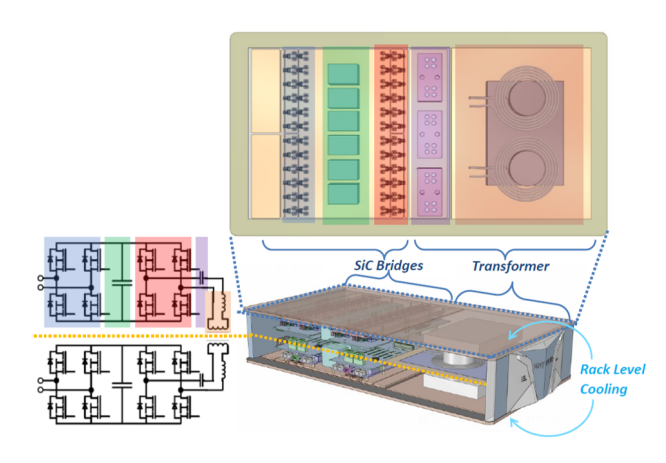


Fig. 1 PEBB half-substrate with heat-generating components labeled. Image courtesy of Virginia Tech Center for Power Electronics Systems (CPES) [6].

via indirect liquid cooling. The findings serve as a baseline for future design iterations and provide a working cooling solution for usage in planned experimental testing of the PEBB.

This paper begins with an overview of the current PEBB design and a review of transformer cooling methods commonly seen in literature. Following this, a heat-pipe-based cooling solution is developed through component-level thermal and electromagnetic simulations. Lastly, the proposed solution is integrated into a half-PEBB thermal simulation for coupled analysis with the current cold plate design.

Background

PEBB. The current iteration of the PEBB occupies an external footprint of 550 mm x 300 mm x 100 mm, and, as stated earlier, must have a total carried weight of under 16 kg [6]. These two requirements are derived from a primary design goal of making the PEBB easy to handle for a single person. Current estimates for the PEBB have a unit weight of 15 kg; however, it is key to note that this weight does not include any in-unit cooling hardware, leaving a maximum of 1 kg for any required additional components [4].

Within the PEBB are two identical halves consisting of electronic components mounted onto a multi-layer common substrate. The components driving the heat losses of the unit are the MOSFET switches, also referred to as SiC Bridges, and the high-frequency transformer, with a combined worst-case heat load of approximately 11 kW for the entire unit. Figure 1 shows the internals of the PEBB with these heat-generating sections highlighted.

MOSFETs. Contributing the highest percentage of heat generation within the PEBB are the 96 SiC MOSFET switches located on the inner-most surface of the common substrate. The location and organization of the SiC MOSFET switches, split between the two half-substrates, can be seen in Fig. 1. Each MOSFET switch is estimated to produce 100 W of waste heat under worst-case conditions, which, when applied to all 96 switches simultaneously, generates up to 9.6 kW of heat that must be conducted through the common substrate [6].

Transformer. The other critical source of heat generation within the PEBB is the high-frequency transformer. The current iteration of transformer is a 100 kW variant, and uses a 3F36 ferrite core with a half-core volume of 110 mm x 55 mm x 65mm. The two core halves are separated by a 3 mm thick mica sheet. For the coils, an overall 8 AWG litz wire with 5x5x3/56/44 strand configuration and an outer polyurethane nylon jacket to 0.211" OD is used. A

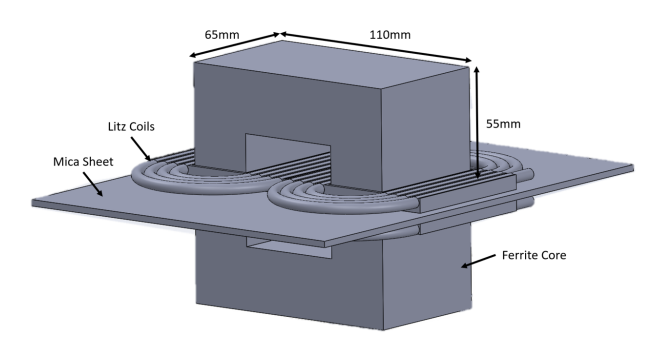


Fig. 2 Current PEBB transformer, Virginia Tech Center for Power Electronics Systems (CPES) [3,4]

visual representation of the transformer geometry and assembly is shown in Fig. 2 [3].

Experimental testing through open-circuit and short-circuit tests of this design resulted in an observed 400-480 W of core heat losses and 144 W of coil heat losses respectively [4]. For the core, the maximum temperature limit going forward will be 100°C based on the exponentially decreasing efficiency of the ferrite material over this value [7]. The coils are bound by the melting temperature of the outer polyurethane nylon jacket, resulting in an upper temperature limit of 155°C [8].

As identified in a previous thermal analysis of the PEBB, the transformer poses a significant challenge due to the previously mentioned limitations in cooling approaches and the geometry of the current design [5]. The transformer currently lacks sufficient access to the heat sink located on both the top and bottom faces of the PEBB unit. As a result, this study will primarily focus on developing a supplementary cooling solution for the transformer and validating all proposed thermal management hardware through PEBB-scale simulations.

Common Substrate. The common substrate forms the base of the PEBB both functionally and structurally, acting as the mounting interface for all components while providing mechanical integrity for the unit. The multi-layer build consists of alternating sheets of copper and an organic direct-bonded copper substrate (ODBC), a design which balances both voltage insulation and heat spreading from the MOSFETs and transformer [4]. With the cold plate in contact with the outer-most layer of copper, all heat generated during PEBB usage will flow through the multi-layer substrate to the rack-mounted cold plates.

Transformer Cooling Literature Review. The cooling of a transformer is crucial to its operation as overheating components can lead to drops in performance and cause damage. Over the decades, cooling methods of varying effectiveness and effort have been developed to meet the rising capabilities of newer builds. Transformers fall into one of two categories based on their cooling methods: the "dry" type and the "wet" type.

The term "dry" refers to transformers that are not directly cooled by a liquid medium, and typically involves air cooling of both the core and coils. Some low-voltage transformers are capable of being cooled through pure natural convection, relying on the buoyancy-driven circulation around the components to maintain acceptable temperatures [9]. For higher voltages and frequencies, however, greater heat transfer coefficients are needed to remove the larger waste heat generated. A common solution is to use forced-air cooling via fans to increase the heat transfer to the air, as shown by Chen et al. in the design of a 200 kHz, medium-voltage transformer [10]. A key feature to note in this design is the "potting" of the coils in epoxy, which is a consequence of the electrical insulation requirements of transformers at these higher voltage levels. The authors note that epoxy is typically selected for

this purpose due to its compromise between electrical insulation and thermal conductivity, since the material becomes a source of thermal resistance between the heat generating coils and air-cooled surface. Warzoha and Fleischer [11] investigate cooling of a universal transformer for terrestrial grid applications using a finned heat pipe array.

Another example of a dry-type transformer can be seen in the design of a high-frequency, medium-voltage transformer by Wang et al. [12]. In this design, the authors explored potting the entire transformer in epoxy and directly attaching it to an air-cooled heat sink on one surface. Rather than cool the transformer directly, air is passed across a finned heat sink such that all the heat must pass through the epoxy medium. The smaller size of this transformer made potting the entire assembly feasible, compared to only potting the coils as is done in other designs. Through both simulation and experimental results, this study was able to demonstrate the feasibility of cooling a transformer core and coils through an indirect heat sink.

In a recent development of a dry-type transformer, Sharfeldden et al. showcase the direct air-cooling of a medium-voltage transformer with exposed coils [13]. This design forewent potted coils and instead relied on direct forced-air cooling over the exposed winding surfaces. According to the authors, the weight savings granted by omitting the layer of epoxy was necessary to meet the low-mass requirement of the system. Focusing on the cooling of the coils, the paper was able to confirm through experiment that a 50 CFM fan was capable of maintaining coil temperatures under 63°C during 175 A, 286 kHz operations.

In a wet-type transformer, the coils and core are submerged in an oil solution which transfers heat from the components to adjacent heat sinks. Similar to the dry-type variants, oil-cooled transformers can utilize both the natural convection of the coolant fluid as well as forced flow over the components to draw heat away from the core and coils [9]. The use of oil, although effective at cooling, results in a significantly higher overall system mass compared to air-cooled solutions. As a result, larger transformers with weight constraints tend to favor dry-cooling approaches.

Heat Pipe Literature Review. A heat pipe is a device which offers strong heat transfer capabilities through the phase-change of its internal working fluid. These components consist of sealed tubes which circulate the fluid between the liquid and vapor phases. With the heat source applied to one end, the local fluid vaporizes and travels through the pipe to the cooler end of the body, where it then condenses back into liquid and releases the latent heat into the heat sink [14]. The design of the wall-lining wick material enables the capillary action that circulates this cooled liquid back to the heat source, finishing the closed-loop process.

The usage of natural circulation in both the liquid and vapor regimes makes a heat pipe a fully passive component, with the advantages of excellent reliability and long lifespan, as heat pipes do not use any moving parts and require zero maintenance. The extremely effective heat-moving capabilities coupled with this reliability are the main factors behind their extensive usage in aerospace applications, where systems are expected to endure extreme conditions for decades without fault [15]. In addition, heat pipes typically are low in weight and can be bent and reshaped to fit into a system. This robustness is extremely useful in weight- and space-constrained systems which require a low-profile method of removing heat. As an example, Cheng et al. [16] used heat pipes for a lightweight battery thermal management system in electric vehicle applications.

The idea of integrating heat pipes into the thermal management of high-frequency transformers has yet to be developed at the commercial level; however, studies exist that explore the implications of such a configuration. In an early study by Hansen and Chester, the direct integration of heat pipes into a 20 kHz, 1.52 kV transformer was tested and found to decrease the observed maximum temperature by 20°C [17]. While this demonstrates the intuitive expectation that heat pipes would enhance the movement

of heat away from the transformer, a major barrier to their mass implementation is the impact on the electromagnetic performance of the system. For example, magnetic fields generated by the transformer's operations can induce electrical currents on nearby magnetic surfaces, leading to additional heat generation. The impacts of these induced losses in any copper-walled heat pipes placed near a high-frequency transformer could result in a system with higher temperatures than designed if these effects are not properly mitigated. In the same study, Hansen and Chester noted the increase in heat losses in the heat pipe-embedded system, but point out that it did not impede the setup from achieving the previously reported temperature drop. A study by Wrobel tabulated the induced losses on heat pipes when used to cool a high-frequency transformer, with different wick structures as well as envelope materials being evaluated [18]. Those results confirmed the increase in expected induced losses with larger operational frequencies. A notable finding from this study was the increasing growth rate of induced losses at higher transformer Also of note was the impact of switching to frequencies. titanium-walled heat pipes, which resulted in an order of magnitude lower losses compared to the standard copper-walled variants.

Heat Pipe Solution Design

In order to cool the PEBB transformer under study, the concept of supplementing a cold plate heat sink with forced air cooling was modeled first, based on a known experimental setup. This serves as both a validation of the modeling and simulation approach as well as a reference for later proposed cooling solutions. After the description of the baseline study, this paper focuses on the development of a heat-pipe-based cooling solution through an iterative design process.

Baseline Assumptions. The construction of the transformer model is based on the geometry and features provided by Sharfeldden [3] and outlined above. The thermal conductivity values of relevant materials are included in Table 1, which also includes additional materials that will be introduced in later heat pipe design sections. Manufacturer's specifications for Ferrite 3F36 provide a range from 3.5 to 5 W/m-K due to inconsistencies in the material properties across multiple samples; therefore, a value of 3.5 W/m-K is used in the simulations in this paper as a conservative estimate. The effective radial thermal conductivity of the exact litz wire construction used for the PEBB transformer was determined using analytical and experimental methods [19].

Heat pipes are modeled as solid rods with a constant, high thermal conductivity that captures the nearly isothermal behavior of the device without requiring the modeling of the multi-phase internal cavity. Following the modeling guidance of Advanced Cooling Technologies (ACT) [14], the thermal conductivity is selected such that a conservative temperature gradient of approximately 5°C is maintained across the length of the heat pipe. The exact value of conductivity varies since changing the heat flow through a heat pipe changes the temperature difference. Each case that was simulated used a heat pipe thermal conductivity value between 10,000 and 15,000 to maintain this desired temperature delta.

The core was modeled with a constant, uniform distribution of heat generation. Its conservative thermal conductivity estimate was applied as an isotropic value across the entire volume. The litz coils were also modeled as uniform volumetric heat sources; however, their thermal conductivity was split into radial and axial components to account for the construction of the wire. Heat transfer along the coil is dominated by heat transfer along the copper strands, and thus the thermal conductivity in the axial direction is set equal to that of solid copper. In the radial direction, an effective thermal conductivity is used based on analytical estimates and experimental results, described in detail in [19], which account for the thermal resistance between individual wires in the bundle.

Table 1 Thermal Conductivities for the PEBB Transformer Thermal Model

Part	Material	Thermal Conductivity <i>k</i> (W/m-K)
Core	Ferrite 3F36	3.5 [19]
Coil (Along Winding, Axial)	Copper	398 [20]
Coil (Radial)	Composite	1.31 [19]
Mica Sheet	Mica	0.3 [21]
Plastic Wireholder	PLA Plastic	0.183 [22]
Ceramic Heat Spreaders	Shapal HiM Soft AlN Ceramic	86 [23]
Aluminum Heat Spreaders	Aluminum 6061	167 [24]
Heat Pipes	n/a	10,000 - 15,000 [19]
Potting Insulation	Epoxy Composite	0.85 [10]

Table 2 Transformer operations loss scenarios

Scenario Name	Total Core Losses (W)	Total Coil Losses (W)
Open Circuit	480	0
Short Circuit	0	144
Combined Loads	480	144

The outer surface of the coils has an area-independent thermal resistance applied to the interface in order to account for the effects of the outer polyurethane nylon sleeve [19]. The impact of interface contact resistance for other component interactions is also considered using this approach. It is assumed that thermal epoxy will be used at all surfaces of contact between the core, mica sheet, and plastic wire holders, as well as any additional components that are added in later design configurations. The area-independent thermal resistance of the thermal epoxy, $R_{epoxy}A$, is estimated using an example manufacturer-reported thermal conductivity and bondline thickness value, $k_{epoxy} = 2.1$ W/m-K and $L_{epoxy} = 1.50e - 5$ m [25] such that

$$R_{epoxy}A = \frac{L_{epoxy}}{k_{epoxy}} = 7.14e - 6 \ Km^2/W$$
 (1)

The primary heat sink for all cases that were modeled is a cold plate; however, to increase the speed of simulations, fluid flow through the cold plates was not modeled. Instead, a standalone transformer model with temperature boundary conditions at the surfaces of contact with the cold plate was used, with the boundary temperatures being pulled from a separate cold-plate-only simulation. This approach allows for a smaller cell count and eliminates the usage of fluid flow solvers, greatly reducing the required computation time and improving the efficiency of model iteration development. A final PEBB-level simulation with full cold-plate fluid flow was later completed to validate the assumptions made in the transformer standalone model; this simulation is described below in the Final Design Half-PEBB Simulation Section.

As stated above, the worst-case heat loss conditions of the core and coils are 480 W and 144 W, respectively. The actual losses can vary depending on the load and usage pattern; however, these maximum values will be applied as a constant heat source for a conservative thermal analysis. Three typical test cases will be used, referred to as the open circuit, short circuit, and combined losses cases, shown in Table 2. All simulation runs will use these cases.

Airflow Cooling Models.

Thermal Model. The configuration for the airflow cooling reference is based on experiments performed by the Virginia Tech Center for Power Electronics Systems (CPES) on the PEBB

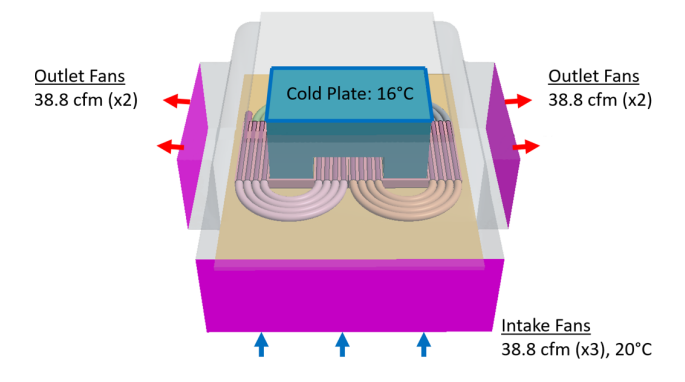


Fig. 3 StarCCM+ thermal model of airflow cooling with boundaries highlighted. The cold plate boundary on the lower core half is not visible.

transformer [4]. In this study, which is shown in Fig. 3, the transformer was placed within a closed box with a 7-fan air cooling system consisting of three front-facing intakes and 4 side-facing outputs. In addition, an off-the-shelf cold plate was used on the upper and lower faces of both core halves to replicate the planned PEBB rack-mounted configuration. An open circuit test was run for 35 minutes with temperature monitoring of the core performed by four surface-mounted thermocouples.

Airflow circulation was accounted for in StarCCM+ through the usage of face boundaries, with the front-facing inlet and side-facing outlets moving 38.8 cfm of air per fan at the presumed ambient temperature of 20°C. Air was modeled as an incompressible fluid with gravity enabled throughout the region. Constant temperature boundaries set to 16°C were defined at the upper and lower core faces to represent the cold plate heat sink. A summary of the relevant boundary conditions can be seen in Fig. 3.

These airflow simulations were each run as a steady steady analysis for a total of 2000 timesteps, which was verified to ensure the convergence of all relevant parameters. The airflow thermal model was successfully correlated with experimental data [19].

PEBB Airflow Reference Scenario. The established air-cooling model was then updated to better reflect the environment of the final PEBB enclosure. Notably, the cold plate temperature was raised from 16°C to 30°C, which is the reference temperature pulled from past thermal modeling of the current PEBB cold plate [5]. The previously used fan configuration and inlet air temperature were reused. In order to fully test the thermal limitations of air cooling, the established conservative thermal conductivity of ferrite $k_{ferrite} = 3.5$ W/m-K was once again applied to the core. The three loss scenarios outlined in Table 2 were simulated, with a summary of maximum temperature results shown in Table 3. A 2D cross-section view of temperatures in the

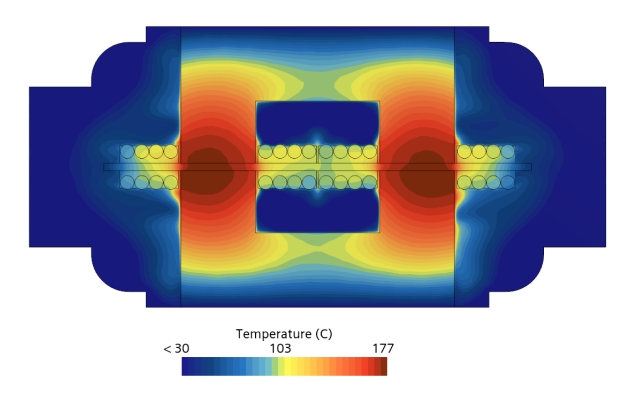


Fig. 4 Cross-section temperatures for the airflow cooling, combined loads scenario

Table 3 Airflow reference scenario maximum temperatures

	Temperature (°C)			
Scenario	Core Maximum	Coil Maximum		
Open Circuit	190.1	76.8		
Short Circuit	47.3	100.0		
Combined Loads	193.3	119.9		

driving design case can be seen in Fig. 4.

These results show that airflow cooling based on the experimental fan configuration is capable of cooling the coils under worst-case operating conditions; however, this methodology fails to cool large regions of the core even with the presence of cold plates on either core outer surface. Sustained transformer operations at core temperatures exceeding 190°C as predicted by the model will further increase the losses experienced by the system, reducing the capabilities of the PEBB unit and possibly leading to a thermal runaway scenario. In addition, the airflow setup modeled would require the design and implementation of an entirely separate air distribution system, taking additional space within the PEBB rack and introducing a potential vulnerability in the event of a fan failure. Based on the results of air cooling, a solution must be designed which simultaneously targets cooling at the inner regions of the core and manages the temperatures of the coils.

Heat Pipe Iteration 1.

Design Solution. With the common substrate already serving as a heat sink thanks to the indirect liquid cooling provided by the cold plate, the idea emerged to utilize more of this cooled surface. By creating alternative paths for heat to travel from the core hot spots to the common substrate, maximum temperatures in the region could be decreased without the need for any additional heat sinks.

Heat pipes were explored for this use case due to their strong ability to move heat and their proven reliability under extreme operating conditions. The initial concept utilizes sixteen heat pipes embedded into aluminum heat spreaders, with each assembly mounted to move heat from the inner regions of the core to the common substrate. Of note is the addition of curved edges on the aluminum heat spreaders in an effort to reduce the intensity of peak electric fields that may occur at sharp metallic corners [26]. In order to extend this new heat sink to the coils, a ceramic heat spreader was designed to bridge the remaining distance while optimizing heat spreading and providing electrical insulation. An image of this concept can be seen in Fig. 5.

Initial heat pipe sizing was completed following an analytical

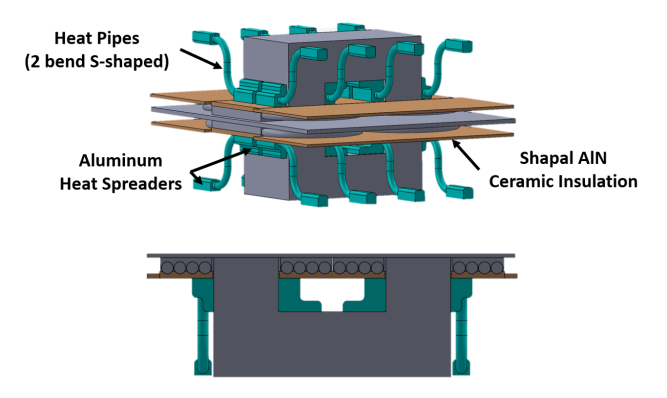


Fig. 5 Isometric view (top) and cross-section view (bottom) of PEBB transformer with heat pipe, iteration 1

method outlined by a well-known distributor, Advanced Cooling Technologies (ACT) [27]. The calculations [19] estimated the need for sixteen 100 mm long, 5 mm diameter copper-water heat pipes. These heat pipes feature two 90° bends with a 15 mm bend radius. At both ends of the heat pipe, 20 mm of length are embedded into aluminum heat spreaders which are designed to maximize the contact area with both the heat sink and heat sources. For this initial design iteration, a basic rectangular prism shape was chosen with the intention of later optimizing for heat spreading and weight reduction. In addition to the embedded heat spreaders, two aluminum spreaders were also placed across the central gaps between core legs.

Serving as both the electrical insulation and heat spreading medium for the high-frequency coils is the ceramic material Shapal HiM Soft Machinable Aluminum Nitride (AlN) [23]. In addition to possessing the strong electrical insulating properties characteristic of ceramic materials, this variant also has a relatively high thermal conductivity of $k_{ceramic} = 86$ W/m-K (interpolated at 100° C), enabling effective heat spreading from the heated coils. This material was chosen due to its ability to be machined, contrary to the brittle nature of typical ceramics and allowing for the design of custom profiles for better integration with the coils and heat pipes. The material's dielectric strength of 65 kV/mm means that just 2 mm of thickness provides insulation against up to 130 kV, meeting and exceeding the BIL test voltage for this transformer [3].

A close-up of the ceramic design can be seen in Fig. 6. The coil-facing surface has a curved profile to increase the area of contact with the coils, improving heat transfer between the two. Although effective, this feature also increases the cost to manufacture the component. In an attempt to balance performance with cost, only the sections of ceramic aligned with the straight sections of coil feature this profile; the remaining ceramic pieces are planar sheets that serve only as electrical insulation. This trade-off is feasible due to the strong heat transfer axially along the coils to the cooled sections. Higher temperatures are expected to appear in the curved sections furthest from the ceramic interfaces. Lastly, a 3D-printed PLA plastic wire holder is used to secure the coils to the mica sheet; this plastic is selected due to its low weight, ease of manufacturing, and current usage in prototype PEBB transformer setups.

Thermal Model. The heat pipe design iterations were simulated in StarCCM+ using similar modeling techniques as in the previous cases; however, all airflow was removed from the simulation domain. The resulting models eliminated convection cooling for the core and coils, requiring all heat to be transferred by conduction to the cold plate heat sink. Radiation was also neglected in these simulations. These conservative assumptions placed additional stress on the heat pipe solutions, while also removing the need for a fluid flow solver and thus greatly reducing simulation times. The only heat sink modeled was the cold plate surface, which is

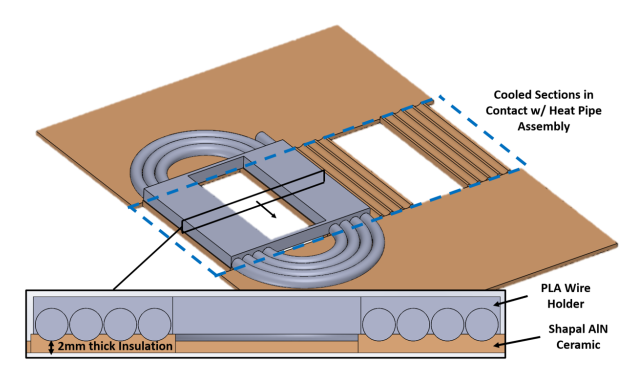


Fig. 6 Transformer coils with ceramic insulation. Second set of coils are hidden.

Table 4 Thermal and weight performance summary: heat pipe iteration 1

	Temperature (°C)			
Scenario	Core Maximum	Coil Maximum		
Open Circuit	84.2	40.3		
Short Circuit	36.6	79.0		
Combined Loads	88.4	86.2		
Temperature Limits	100	155		
Total Added Weight	0.75 kg (1.66 lb)			

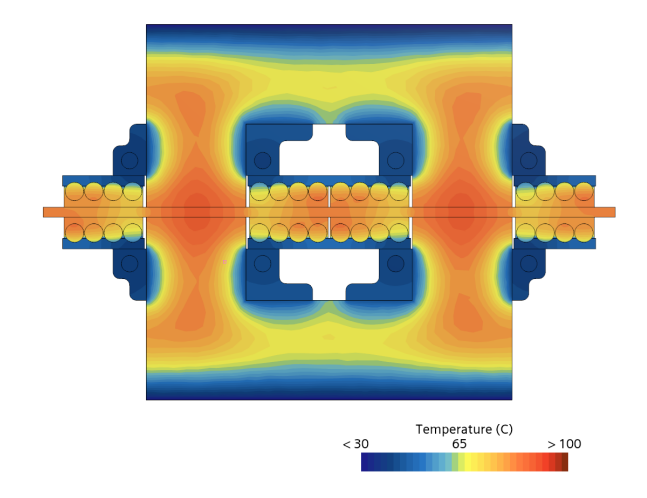
assumed to be at 30°C.

Thermal Results and Analysis. A summary of the maximum core and coil temperatures seen with this configuration can be found in Table 4. The highest temperatures in all three loss scenarios are well within design limits and showcase the successful extension of the cold plate heat sink. The use of aluminum heat spreaders effectively pulled heat from the central regions of the core, as shown in Fig. 8, top. Figure 7, bottom, shows the successful management of coil temperatures well below their design limit of 155°C despite only the straight sections of coil being in contact with the extended heat sink. These acceptable thermal results required the addition of 0.75 kg of mass for the heat pipes, aluminum heat spreaders, and ceramic insulation pieces.

Heat Pipe Iteration 2.

Design Changes. With the first design providing the proof of concept, the next iteration aimed to maintain acceptable temperatures while also introducing the electromagnetic analysis. The changes made are focused on the transformer-side heat spreaders, which were changed from aluminum blocks to AlN ceramic variants of similar geometry. With the transformer operating at high frequencies (430 kHz), the induced losses in any aluminum near the coils would likely lead to significant heat generation, requiring a change in material. AlN ceramic acts as an electrical insulator in addition to its high voltage tolerance, and in a study by Wrobel et al. [28] was experimentally proven to have negligible induced heat generation when near high-frequency electronics. Due to near-zero magnetic flux leakage at their current positions, the common substrate-side heat spreaders were left as aluminum.

The slightly higher density of this specific AlN compared to aluminum (2.88 g/cm³ vs 2.7 g/cm³) was compensated for by slightly reducing the overall footprint of the new ceramic heat spreaders. Overall, this second iteration reduced the weight of the added hardware by 12 g, giving a new total mass estimate of 0.74 kg.



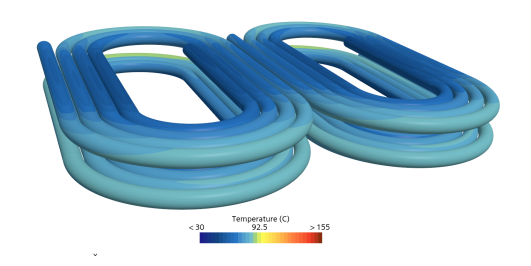


Fig. 7 Cross-section temperatures (top) and coil surface temperatures (bottom) for heat pipe iteration 1, combined loads scenario

Table 5 Thermal and weight performance summary: heat pipe iteration 2

	Temperature (°C)			
Scenario	Core Maximum	Coil Maximum		
Open Circuit	89.3	40.3		
Short Circuit	36.8	80.2		
Combined Loads	93.7	87.1		
Total Added Weight	0.74 kg (1.63 lb)			

Thermal Simulation, Results and Analysis. Thermal simulations for the second design iteration were run using the same properties and conditions outlined for Heat Pipe Iteration 1 above. A summary of the maximum core and coil temperatures seen with this second configuration can be found in Table 5. Changing the heat spreaders from aluminum to ceramic AlN was found not to have a major effect on the thermal management of the core and coils, with hot-spot temperatures still below maximum limits despite a 5°C increase in the case of the core.

Electromagnetic Analysis. Electrical analysis focused on modeling the effects of high-frequency coil operations on the copper-walled heat pipes. A quarter model of the PEBB transformer with the proposed heat pipe configuration was built in StarCCM+ using the material properties in Table 6. With the exception of ferrite, the properties were based on the StarCCM+ local material database. Since the AlN ceramic is expected to have negligible heat losses, only the heat pipes were modeled.

The coil winding was modeled as 4 separate concentric loops, with a total combined electrical resistance of $R_{coil} = 4.53e-3~\Omega$. AC current through these coils was simulated at a magnitude of

Table 6 Electromagnetic properties for the PEBB transformer/heat pipe magnetic analysis

Material	Electrical Conductivity (S/m)	Magnetic Permeability (H/m)
Air	8.00e-15	1.26e-6
Copper	5.96e7	1.26e-6
Ferrite 3F36	1.23 [7]	2.01e-3 [7]

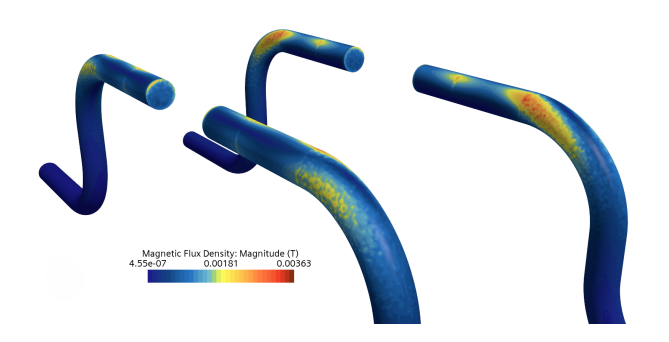


Fig. 8 Magnetic flux for 430 kHz operations of heat pipe iteration 2

45 A and at the current transformer design frequency of 430 kHz. The heat pipes were modeled as hollow due to the negligible heat generation through the internal working fluid. Since electrical currents are only generated in a thin layer at the surface, the heat pipe model and mesh were built to be one skin depth thick at 430 kHz, reducing the cross-sectional area and capturing the higher electrical resistance that will be present.

The transient run revealed maximum induced heat generation of 1.91 W per heat pipe for both the side and middle variants. When multiplied over the entire transformer, this results in 30.56 W of additional heat generation, nearly equivalent to an additional coil winding. A cross-section view of the resulting magnetic field can be seen in Fig. 9. Note that the field is nearly vertical at the core wall.

In order to better analyze heat pipe losses in this configuration, the simulation was rerun for different transformer operational frequencies. For each run, the wall thickness of the heat pipe model was updated to match the respective skin depth at that frequency. Results of this study can be seen in Fig. 10, and show a linear trend between the two parameters in the range of frequencies tested.

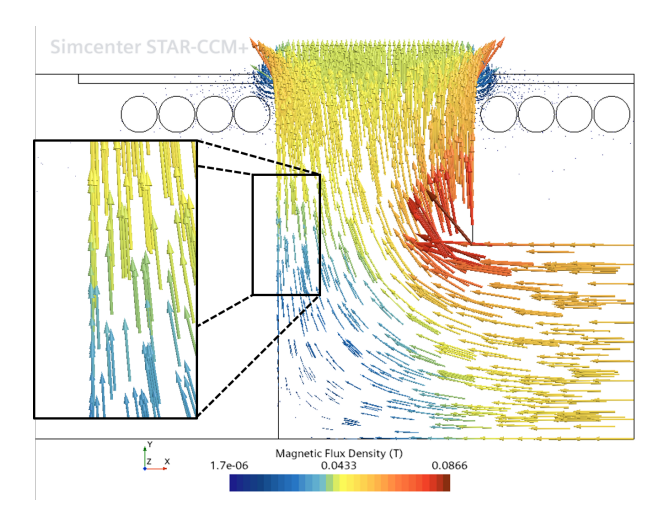


Fig. 9 Core magnetic flux field for a given time step from the quarter transformer model

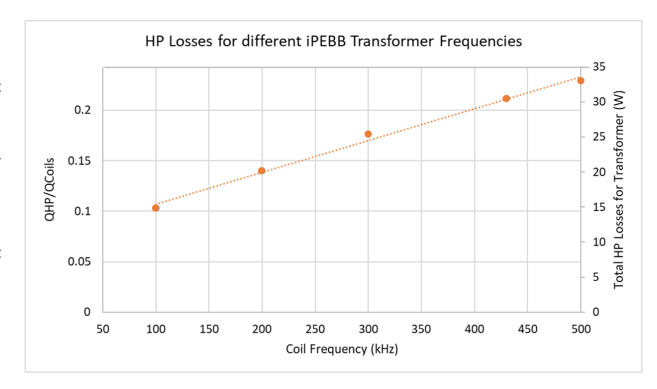


Fig. 10 Heat pipe (HP) heat losses for S-shaped configuration at different PEBB operational frequencies. Left axis shows the ratio of induced HP losses (QHP) to coil losses (QCoils); right axis shows total induced HP losses.

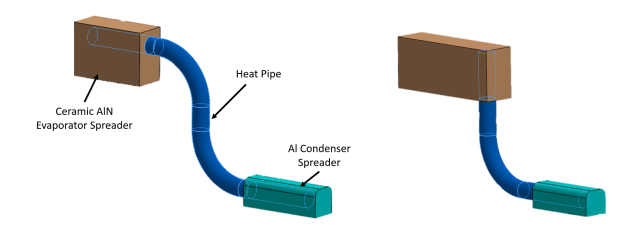


Fig. 11 S-shaped 2-bend heat pipe (left) and L-shaped 1-bend heat pipe (right)

Heat Pipe Iteration 3.

Design Changes. The next design explored adjusting the orientation of the heat pipes to better align with the direction of the local magnetic field, with the aim of reducing heat pipe magnetic flux and generated losses. The magnetic field follows the loop created by the two transformer core halves, with any flux leakage into the surrounding air running parallel to the outer core surface. The proposed geometry replaced the 2-bend, S-shaped heat pipes with a 1-bend, L-shaped configuration that mostly parallels the core side surfaces. These shorter, 75 mm heat pipes replaced the previous 100 mm models while retaining the same diameter of 5 mm. The geometry of the core meant that the middle heat pipes had to be shifted to outside the central core gap, requiring larger ceramic heat spreaders. This resulted in an increase in heat spreader volume and subsequent weight, raising the total mass estimate of iteration 3 to 0.77 kg. The side-mounted heat pipes were able to remain in roughly the same location as iteration 2, with the ceramic heat spreaders modified slightly to retain a similar

This configuration offers the advantage of reducing the number of heat pipe bends required and allowing for the usage of shorter variants, both of which increase the heat capacity of the heat pipes. A side-by-side comparison of the two heat pipe options for the middle region can be seen in Fig. 11.

Thermal Simulation, Results and Analysis. Replacing the aluminum spreaders with a ceramic of lower thermal conductivity was expected to slightly increase hot-spot temperatures across the core; however, the largest impact was caused by the repositioning of the middle heat pipes outside of the core gap. As seen in Fig. 12, moving the middle heat pipes from their previously close location next to the core surface significantly raised the temperatures at that interface, reducing the effectiveness of the added heat sink. As a result, hot-spot temperatures increased, with those of the core reaching just above the 100°C limit; see Table 7. In addition to the

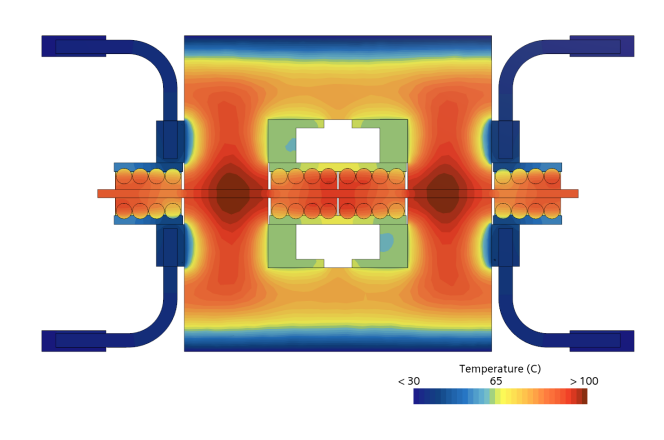


Fig. 12 Cross-section temperatures for heat pipe iteration 3, combined loads scenario

Table 7 Thermal and weight performance summary: heat pipe iteration 3

	Temperature (°C)			
Scenario	Core Maximum	Coil Maximum		
Open Circuit	95.0	49.3		
Short Circuit	40.8	82.6		
Combined Loads	102.3	95.8		
Total Added Weight	0.77 kg (1.71 lb)			

reduced thermal performance, the stretching of the middle ceramic spreaders also raised the weight of this configuration to 0.77 kg, the heaviest of the currently explored designs.

Electromagnetic Analysis. The high-frequency analysis of the heat pipe configuration followed the same setup and approach of iteration 2, with the updated model shown in Fig. 13. This iteration's heat pipe positioning and orientation was selected with the goal of minimizing magnetic flux through the heat pipes while still retaining effective cooling.

At 430 kHz, this run revealed maximum induced heat generations well below those of iteration 2, with the side heat pipes seeing the largest decrease from 1.91 W to 0.37 W per heat pipe. Although lower than in iteration 2, the middle L-shaped heat pipes still experienced approximately 0.80 W per heat pipe, giving a configuration total of 9.36 W for the entire transformer.

Just as for the S-shaped heat pipe configuration, this simulation

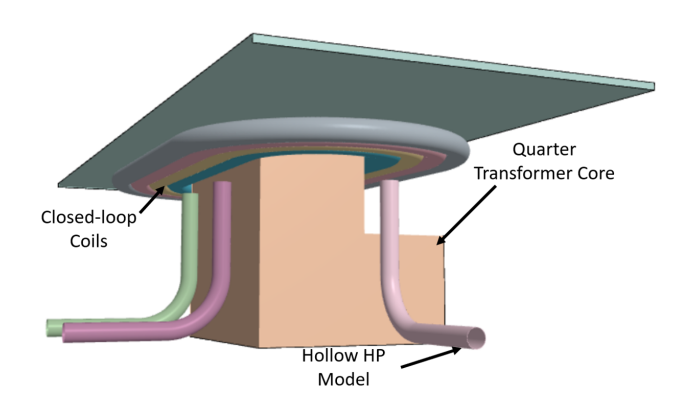


Fig. 13 Quarter model of PEBB transformer heat pipe, iteration 3



Fig. 14 Magnetic flux for 430 kHz operations of heat pipe iteration 3

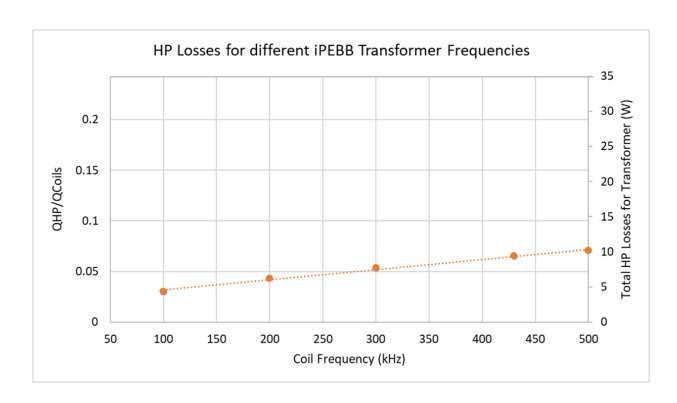


Fig. 15 Heat pipe (HP) heat losses for L-shaped configuration at different PEBB operational frequencies.

was rerun at different transformer operational frequencies with the wall thickness of the heat pipe model updated to match the respective skin depth at each frequency. Results for the dual L-shaped heat pipes can be seen in Fig. 15, and again show a linear trend between the two parameters. The left axis shows the ratio of induced heat-pipe losses to coil losses, and the right axis shows total induced heat-pipe losses for the transformer.

Heat Pipe Final Iteration.

Design Changes. The goal of the final iteration was to combine the advantages of iterations 2 and 3 in order to achieve acceptable thermal performance while minimizing the induced losses within the heat pipes due to high-frequency operations. Although the S-shaped heat pipes experienced higher magnetic flux, and in turn higher induced losses, iteration 3 showed that removing these from the center opening of the transformer increased core hot-spot temperatures to the point of noncompliance. Furthermore, the use of S-shaped heat pipes in the middle gap reduced the size and weight of ceramic spreader required compared to the L-shaped variant. Therefore, it was decided to utilize the 100 mm long, S-shaped heat pipes in the middle gap in addition to 75 mm long, L-shaped heat pipes on the outer sides of the core, as shown in Fig. 16. Previous results showed that substituting L-shaped heat pipes for the transformer sides reduced induced losses by 81% when compared to S-shaped heat pipes in this region without severely reducing heat transfer performance.

Thermal Simulation, Results and Analysis. Simulation results showed that utilizing this hybrid heat pipe configuration restored the nearly symmetrical dual heat sinks on either side of the core pillars. As shown in Fig. 17, restoring the S-shaped heat pipes in the central gap helped reduce core hot spots located near the mica sheet back below the 100°C limit in the combined loads scenario. Thermal and magnetic performance summaries are shown in Tables 8 and 9 respectively. When compared to the

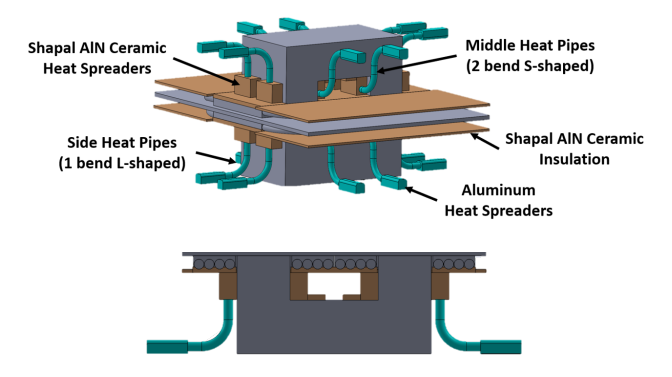


Fig. 16 Isometric view (top) and cross-section view (bottom) of PEBB transformer with the final heat pipe iteration

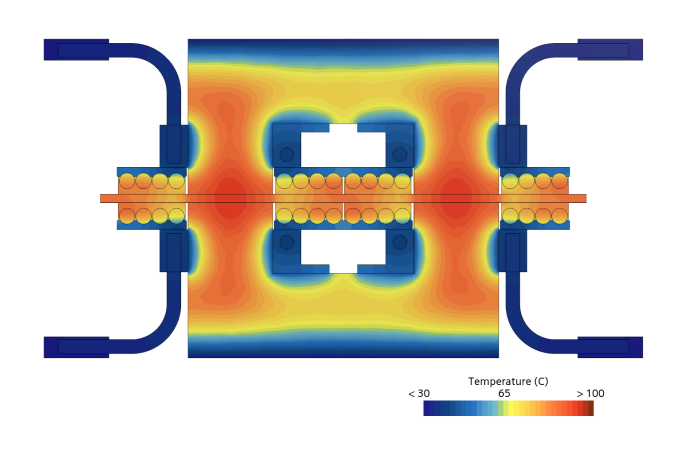


Fig. 17 Cross-section temperatures for heat pipe final iteration, combined loads scenario

airflow baseline results in Fig. 4, this is a considerable improvement (note difference in thermal scale). In addition, replacing the relatively large ceramic heat spreaders of the L-shaped middle heat pipes reduced the total weight of the configuration to just 0.73 kg.

Induced Losses. Since this configuration is a hybrid of iterations 2 and 3, the relevant results from the previous electromagnetic studies were reused for the heat pipe positions and orientations chosen.

The standalone thermal model was then rerun with these estimated heat pipe induced losses added. All were modeled as volumetric heat sources and were localized on the sections of heat pipe that saw the majority of the induced losses. These aligned roughly with the areas of heat pipe with high magnetic flux density seen in Fig. 8 and Fig. 14. Heat flow values through each heat pipe are recorded for this final run in Table 10, alongside adjusted values Q_{max} which consider the roughly 5% reduction in heat

Table 8 Thermal and weight performance summary: heat pipe final iteration

	Temperature (°C)		
Scenario	Core Maximum	Coil Maximum	
Open Circuit	89.7	42.2	
Short Circuit	37.3	81.0	
Combined Loads	94.4	88.2	
Total Added Weight	0.73 kg (1.61 lb)		

Table 9 Magnetic performance summary: heat pipe final iteration

Component	Peak Heat Generation (W)
L-shaped Side HP S-shaped Middle HP	0.37 1.91
Total Transformer (x8 side HPs, x8 middle HPs)	18.24

Table 10 Final iteration heat flow at 430 kHz AC operations (with adjusted Q_{max} including 30% safety factor and bends)

	(W)				
		Component	Q_{sim}	Q_{max}	Qmax/Capacity
		HP 1	21.3	28.8	0.488
	≽	HP 2	21.2	28.6	0.484
S	59	HP 3	21.6	29.2	0.495
Side HPs		HP 4	21.5	29.1	0.493
de	cit	HP 5	21.6	29.2	0.495
Side F Capacity:	HP 6	21.5	29.1	0.493	
	$\ddot{\mathbb{C}}$	HP 7	21.2	28.6	0.485
		HP 8	21.3	28.8	0.488
Middle HPs Capacity: 44 W		HP 9	30.0	42.1	0.956
	HP 10	30.6	42.8	0.973	
	HP 11	30.2	42.3	0.962	
	HP 12	30.4	42.6	0.969	
	HP 13	30.2	42.3	0.962	
	фа	HP 14	30.6	42.8	0.973
_	$\ddot{\mathbb{C}}$	HP 15	30.4	42.6	0.969
		HP 16	30.0	42.1	0.957

transfer capability per 90° bend on each heat pipe as well as a 30% safety factor [29]. Even after applying these factors, the maximum heat loads do not exceed the heat pipe capacities, which take into account pipe geometry and approximate operating temperature.

Final Design Half-PEBB Simulation

Design and Thermal Model. A half-PEBB thermal model was built in StarCCM+ using the common substrate and cold plate designs outlined previously in the Background Section. Due to the symmetry of the PEBB, a half model with an applied symmetry boundary condition allowed for the simulation of the whole PEBB at a fraction of the computational cost. This model employed the final heat pipe cooling configuration from the Heat Pipe Final Iteration Section. In addition to the transformer thermal modeling, this model included the 100 W of heat generation per MOSFET, and modeled the full cold plate with fluid flow. A view of this model can be seen in Fig. 18.

In addition to the usage of ceramic heat spreaders, modifications were made to the common substrate to further prevent the creation of electrical paths to ground from the transformer due to the addition of heat pipes. The top layer of copper under the transformer was sectioned in a similar manner to the MOSFET side of the PEBB. This step serves as an extra precaution to ensure electrical insulation between any two heat pipe legs, as each copper island is directly mounted to a dielectric ODBC layer. The details regarding the exact design can be modified; however, the proposed configuration offers weight savings of 0.44 kg between both common substrates, offsetting the added weight of the heat pipe/ceramic solution to only have a net weight of 0.29 kg.

As in the standalone transformer models, the half-PEBB model was built without any airflow present, removing convection cooling for the transformer and MOSFETs and forcing all heat to be removed by the proposed cooling hardware. Fluid flow through

the cold plate was modeled using the expected baseline inlet water temperature of 22°C and mass flow rate of 0.370 kg/s [30]. This replaces the previously set boundary condition of a 30°C constant surface at the top layer of the common substrate.

Several new interfaces were modeled using an area-independent thermal resistance applied to their respective faces. For the MOSFETs, the effect of the sintered connection to the common substrate was captured using estimated properties of a 22% porous silver sample, with a thermal conductivity of $k_{sinter}=151.6$ W/m-K and interface thickness of $L_{sinter}=48~\mu m$ [31].

$$R_{sinter}A = \frac{L_{sinter}}{k_{sinter}} = 3.17e - 7 \ Km^2/W \tag{2}$$

The thin layers of ODBC sheets and the thermal interface material PGS sheets were also modeled using an area-independent thermal resistance, rather than having their geometry physically represented. Using an effective interface resistance captured the thermal resistance through the layer without the need to mesh the thin surfaces, which would have added a large number of cells to the overall model. The capturing of heat spreading within these layers is also insignificant due to their poor thermal conductivities and extremely thin profiles. Using the known thicknesses (L_{ODBC} , L_{PGS}) and thermal conductivities (k_{ODBC} , k_{PGS}) of these layers gives the following values [4,32]:

$$R_{ODBC}A = \frac{L_{ODBC}}{k_{ODBC}} = \frac{(3.50e - 5) \ m}{0.7 \ W/mK} = 5.00e - 5 \ Km^2/W \ (3)$$

$$R_{PGS}A = \frac{L_{PGS}}{k_{PGS}} = \frac{(1.96e - 4) \ m}{1.38 \ W/mK} = 1.42e - 4 \ Km^2/W$$
 (4)

Thermal Results and Analysis. In addition to the baseline inlet water temperature of 22°C, another scenario in which chilled water is utilized instead of deionized water was run. Using a chilled loop would provide a cooler inlet water temperature of 7°C; however, it would require the PEBB to be fully electrically isolated, which is still being studied. Results from the two cases are listed in Table 11. In both cases, the temperature change seen between cold plate inlet and outlet ports was 3.3°C and the simulated pressure drop across the cold plate was 675.5 Pa.

Thermal steady-state results for 22°C inlet deionized water flow are shown in Figures 19, 20, and 21. Hot-spot temperatures for the half-PEBB model are approximately 5°C higher than the standalone model, which can possibly be attributed to the reduced heat spreading of the now trimmed common substrate top layer. Temperature gradients within and across the transformer are consistent, however, and reveal identical hot-spot locations that still fall below the 100°C core and 155°C coil limits. Looking at the MOSFETs confirms heat overlap between subsequent MOSFET switches; however, temperature estimates confirm the effectiveness of the heat spreading provided by the common substrate design. Maximum MOSFET temperatures remain below the 150°C limit.

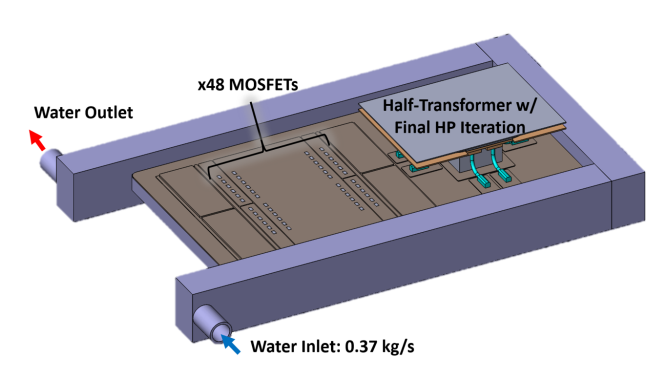


Fig. 18 Half-PEBB model with final transformer heat pipe design integrated

Table 11 Thermal and weight performance summary: half-PEBB final heat pipe design

Cold Plate Inlet Water Temperature (°C)	Maxin	num Tem	perature (°C)
	Core	Coils	MOSFETs
22.0	99.7	93.2	144.6
7.0	84.7	78.2	129.6
Temperature Limits	100	155	150
Net Added Weight	(0.29 kg (0.63 lb)

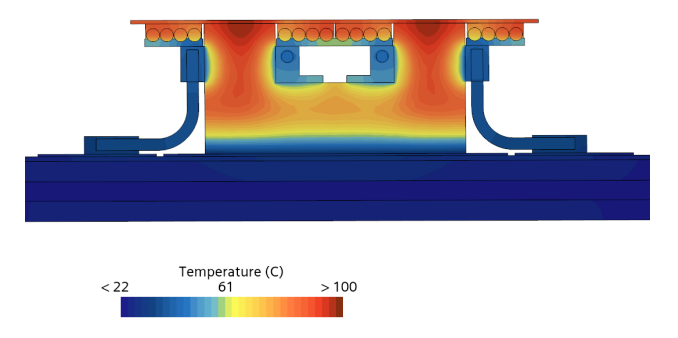


Fig. 19 Transformer cross-section temperatures for the half-PEBB final heat pipe model, combined loads scenario, at steady state with an inlet water temperature of 22°C

Conclusions and Future Work

In this study, the usage of heat pipes to provide supplementary cooling to a high-frequency transformer was studied and analyzed. First, thermal models of the transformer were built in StarCCM+ and used to simulate worst-case loss scenarios under various cooling solutions. Airflow cooling was modeled based on available test data, and was used to provide baseline temperature results for the PEBB transformer. Multiple heat pipe configurations were then modeled and used to provide a supplementary path for heat to flow from the hot-spot regions of the transformer to the cooled common substrate. Electromagnetic simulations were used to model the impact of high-frequency coil operations on the proposed heat pipe configurations. The final heat pipe configuration was then integrated into an PEBB-level simulation with the cold plate fluid modeled. Results showed that the final heat pipe configuration was capable of maintaining transformer component temperatures below their acceptable limits, while not producing induced heat pipe losses exceeding their design heat load capacities.

The final design utilizes 16 heat pipes embedded in aluminum nitride ceramic heat spreaders on one end, which are directly mounted to the "legs" of the transformer core, and to aluminum heat spreaders on the other end, mounted to the common substrate surface. AlN ceramic fixtures are used to provide direct contact between these heat spreaders and the litz wire coils. The high voltage insulation of the transformer coils, minimization of high-frequency induced heat generation in the copper-walled heat pipes, and prevention of any additional loops of electric current flow between the transformer and ground were all considered and mitigated in the design process.

Thermal simulations of the final design integrated with the PEBB model predicted temperature hot spots of 99.7°C for the transformer core, 93.2°C for the transformer coils, and 144.6°C for the MOSFET switches when cooled by a flow rate of 0.37 kg/s of deionized water at 22°C through the current cold plate design. All of these maximum temperatures fall within the temperature limits. For the MOSFETs, this includes a safety factor of 30°C. These results were attained for an PEBB with a constant 9.6 kW

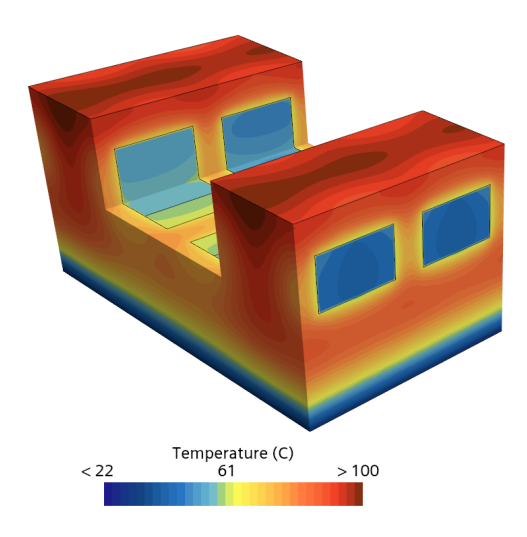


Fig. 20 Transformer core surface temperatures for the half-PEBB final heat pipe model, combined loads scenario, at steady state with an inlet water temperature of 22°C

of MOSFET losses across 96 switches, 480 W of transformer core losses, and 144 W of coil winding heat generation. The positioning of 2-bend, S-shaped heat pipes within the middle core gap and 1-bend, L-shaped heat pipes at the outer side surfaces resulted in within-limit heat flow values through each component. Magnetically, simulations predicted an additional 18.24 W of heat generation across the 16 heat pipes due to the nearby magnetic flux leakage. Accounting for all transformer heat loads in addition to induced loads and a 30% safety factor, this results in a maximum load of 42.8 W through any heat pipe, which falls within capacity of the selected heat pipe size. Due to the isothermal behavior of heat pipes when operating under their maximum heat capacity, these induced losses did not affect the temperatures predicted within the transformer. The proposed hardware was predicted to weigh 0.73 kg; however, with reductions to the current copper common substrate footprint, the net weight addition to the PEBB was reduced to 0.29 kg.

These results, although promising, require further analysis for implementation in the PEBB. Notably, experimental measurements of the induced heat pipe losses and resulting temperatures must be gathered at the target design frequency in order to validate simulation predictions. Various conservative assumptions were made throughout the modeling process in order to reduce the risk of the final results; however, with more accurate material properties, the design can likely be optimized for further weight and temperature reductions. The use of Shapal HiM Soft Machinable AlN ceramic was crucial to the design of the proposed solution; however, it must be noted that this is currently a custom-made material, and may prove expensive for usage across thousands of PEBBs needed for a naval ship implementation.

Ultimately, future design changes for the PEBB transformer will require a redesign and analysis of the cooling solution regardless of approach; however, the findings of this paper demonstrate the thermal feasibility for the usage of heat pipes in cooling high-frequency electronics.

Shortening the core to reduce the distance to the common substrate would help with the reduction of hot-spot temperatures in the core. This change would also place the coils closer to the common substrate, reducing the need for heat pipes and opening up coil potting as a possibly viable solution.

As for the heat pipes, there are various steps that can be taken to reduce the impacts of high-frequency operations. Based on similar heat pipe experiments and modeling by Wrobel [18], switching the copper-walled heat pipes to titanium-walled variants

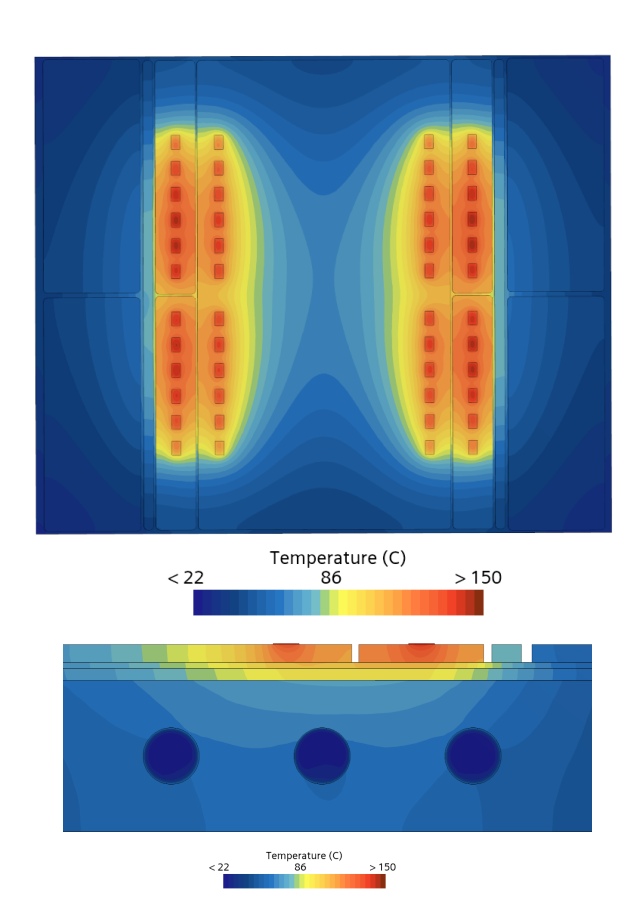


Fig. 21 MOSFET surface temperatures for the half-PEBB model, combined loads scenario, at steady state with an inlet water temperature of 22°C, top and side views

could reduce the effects of the magnetic field by an order of magnitude. In the future, a possible solution could be the usage of ceramic-walled heat pipes, which could render the impacts of induced losses negligible. Research of this technology is ongoing, with heat pipe manufacturer ACT receiving a multi-million dollar grant in late 2023 from the U.S. Department of Energy for the development of this exact concept for usage in transformer cooling [33]. Both ceramic- and titanium-walled heat pipes are likely to be significantly more expensive than the copper-walled heat pipes used here. Another possible area for investigation is polymeric heat pipes, e.g. those designed by Luo et al. [34], which have significant dielectric capabilities.

The usage of heat pipes proposed in this paper successfully cools the PEBB transformer, with minimal added weight, while addressing high-frequency concerns posed by the coil operations. Heat pipe cooling for transformers has the potential to remove the current thermal limitations for weight-constrained power electronics designs, opening up new capabilities for PEBBs, electric vehicle charging, and more.

Acknowledgment

This project is in collaboration with ongoing research by the Virginia Tech Center for Power Electronics Systems (CPES) accomplished by Christina DiMarino, Narayanan Rajagopal, Sharifa Sharfeldden, and Taha Moaz, and building on early development by FastWatt LLC and Ravi Raju.

Approved for public release under DCN# 543-2267-24. The views expressed are those of the authors and do not reflect the official policy or position of the U.S. Department of Defense or the U.S. Government.

Funding Data

- U.S. Office of Naval Research No. N00014-21-1-2124
- U.S. National Oceanic and Atmospheric Administration No. NA22OAR4170126

References

- [1] Petersen, L., Schegan, C., Ericsen, T. S., Boroyevich, D., Burgos, R., Hingorani, N. G., Steurer, M., Chalfant, J., Ginn, H., DiMarino, C., Montanari, G. C., Peng, F. Z., Chryssostomidis, C., Cooke, C., and Cvetkovic, I., 2022, "Power Electronic Power Distribution Systems (PEPDS) Plan," https://www.esrdc.com.
- [2] Rajagopal, N., 2021, "Design of 1.7 kV SiC MOSFET Switching Cells for Integrated Power Electronics Building Block (iPEBB)," Master's thesis, Virginia Polytechnic Institute and State University, Blacksburg, VA.
- [3] Sharfeldden, S., 2023, "Design of a 405/430 kHz, 100 kW Transformer with Medium Voltage Insulation Sheets," Master's thesis, Virginia Polytechnic Institute and State University, Blacksburg, VA.
- [4] DiMarino, C., 2023, "ONR Power Electronics Power Distribution System (PEPDS) Risk Reduction Program Review," Virginia Tech Center for Power Electronics Systems (CPES).
- [5] Hernandez, D., 2023, "Thermal Analysis of Indirect Liquid Cooling for the Navy integrated Power Electronics Building Block," Bachelor's thesis, Massachusetts Institute of Technology, Cambridge, MA.
- Institute of Technology, Cambridge, MA.

 [6] Rajagopal, N., 2020, "Navy Integrated Power Electronics Building Block (Navy iPEBB)." Virginia Tech Center for Power Electronics Systems (CPES).
- [7] Ferroxcube, 2013, Soft Ferrites and Accessories Data Handbook, accessed 2023-05-07, https://www.ferroxcube.com/en-global/download/download/11
- [8] Cooner Wire, Cooner Wire Catalog, accessed 2024-02-06, https://www.coonerwire.com/cooner_catalog_rev9-8.pdf
- [9] Daware, K., "Cooling Methods of a Transformer," accessed 2024-02-29, https://www.electricaleasy.com/2014/06/cooling-methods-of-transformer.html
- [10] Chen, Q., Raju, R., Dong, D., and Agamy, M., 2018, "High Frequency Transformer Insulation in Medium Voltage SiC enabled Air-cooled Solid-State Transformers," 2018 IEEE Energy Conversion Congress and Exposition (ECCE), pp. 2436–2443, doi: 10.1109/ECCE.2018.8557849.
- [11] Warzoha, R. and Fleischer, A. S., 2011, "Thermal Management of a 15 kV/100 kVA Intelligent Universal Transformer," ASME Journal of Thermal Science and Engineering Applications, 3(1), p. 011002.
- [12] Wang, H., Guo, Z., Tayebi, S. M., Zhao, X., Huang, Q., Yu, R., Yang, Q., Li, Y., and Huang, A. Q., 2020, "Thermal Design Consideration of Medium Voltage High Frequency Transformers," 2020 IEEE Applied Power Electronics Conference and Exposition (APEC), pp. 2721–2726, doi: 10.1109/APEC39645.2020.9124264.
- [13] Sharfeldden, S., Raju, R., and DiMarino, C., 2022, "Insulation Design for a Compact, Medium-Voltage Transformer," 2022 IEEE Energy Conversion Congress and Exposition (ECCE), pp. 1–6, doi: 10.1109/ECCE50734.2022.9947979.
- [14] "Heat Pipes 101," Advanced Cooling Technologies, accessed 2024-05-28, https://www.1-act.com/thermal-solutions/passive/heat-pipes/heat-pipes-101/
- [15] Shukla, K. N., 2015, "Heat Pipe for Aerospace Applications—An Overview," *Journal of Electronics Cooling and Thermal Control*, pp. 1–14, doi: 10.4236/jectc.2015.51001.
- [16] Cheng, J., Shuai, S., Zhao, R., and Tang, Z., 2022, "Numerical Analysis of Heat-Pipe-Based Battery Thermal Management System for Prismatic

- Lithium-Ion Batteries," ASME Journal of Thermal Science and Engineering Applications, 14(8), p. 081008.
- [17] Hansen, I. G. and Chester, M. S., 1979, "Heat Pipe Cooling of Power Processing Magnetics," *International Conference on Electric Propulsion*, https://ntrs.nasa. gov/citations/198000030805
- [18] Wrobel, R., 2024, "Analysis of Power Loss in Heat Pipes for Integrated Thermal Management of Next Generation Electrical Machines," Thermal Science and Engineering Progress, 47, p. 102358.
- [19] Hernandez, D., 2024, "Heat Pipes for the Thermal Management of High Frequency Transformers in the Navy integrated Power Electronics Building Block," Master's thesis, Massachusetts Institute of Technology, Cambridge, MA.
- [20] MatWeb, Copper, accessed 2024-02-24, https://matweb.com/search/DataSheet. aspx?MatGUID=9aebe83845c04c1db5126fada6f76f7e&ckck=1
- [21] S and R Optic, Mica, accessed 2024-02-24, https://www.sr-optic.com/Materials/ Mica/
- [22] Spinelli, G., Kotsilkova, R., Ivanov, E., Georgiev, V., Naddeo, C., and Romano, V., 2022, "Thermal and Dielectric Properties of 3D Printed Parts Based on Polylactic Acid Filled with Carbon Nanostructures," Macromolecular Symposia, 405(1).
- [23] Precision Ceramics, Shapal Hi M Soft, accessed 2024-01-10, https://precision-ceramics.com/materials/shapal/
- [24] MatWeb, Aluminum 6061-T6, accessed 2024-02-24, https://www.matweb.com/search/DataSheet.aspx?MatGUID=b8d536e0b9b54bd7b69e4124d8f1d20a&ckck=1
- [25] MasterBond, Thermally Conductive Epoxy Adhesives, accessed 2024-05-24, https://www.masterbond.com/properties/thermally-conductive-epoxy-adhesives
- [26] Stewart, J., Motwani, J., Yu, J., Cvetkovic, I., and Burgos, R., 2022, "Improved Power Density of a 6 kV, 1 MW Power Electronics Building Block Through Insulation Coordination," 2022 IEEE 23rd Workshop on Control and Modeling for Power Electronics (COMPEL), pp. 1–7, doi: 10.1109/COMPEL53829.2022.9829968.
- [27] 2021, "Heat Pipe Design and Modeling Techniques," accessed 2023-09-22, https://www.youtube.com/watch?v=Shisfff7ulM
- [28] Wrobel, R. and Hussein, A., 2020, "A Feasibility Study of Additively Manufactured Heat Guides for Enhanced Heat Transfer in Electrical Machines," IEEE Transactions on Industry Applications, 56(1), pp. 205–215.
- [29] "Bending Heat Pipes, How it Affects Vapor Chambers and Heat Pipes," accessed 2024-07-24, https://celsiainc.com/heat-sink-blog/bending-heat-pipes/
- [30] Chatterjee, A., 2023, "Design and Modeling of Shipwide Navy Integrated Power and Energy Corridor Cooling System," Master's thesis, Massachusetts Institute of Technology, Cambridge, MA.
- [31] Ordonez-Miranda, J., Hermens, M., Nikitin, I., Kouznetsova, V. G., van der Sluis, O., Ras, M. A., Reparaz, J., Wagner, M., Sledzinska, M., Gomis-Bresco, J., Sotomayor Torres, C., Wunderle, B., and Volz, S., 2016, "Measurement and Modeling of the Effective Thermal Conductivity of Sintered Silver Pastes," International Journal of Thermal Sciences, 108, pp. 185–194.
- [32] Padilla, J., Lietch, E., Chalfant, J., and Chryssostomidis, C., 2023, "Impact of Pressure Profile on Contact Resistance using PGS in iPEBB Cooling," Proceedings of the IEEE Electric Ships Technology Symposium 2023, Alexandria, VA, August 1–4, pp. 343–352.
- [33] 2023, "ACT Wins \$5.5m for Five Heat Pipe Projects," accessed 2023-12-01, https://www.eenewseurope.com/en/act-wins-5-5m-for-five-heat-pipe-projects/
- [34] Luo, K., Gross, A. J., Brown, J., Chang, W., and Li, C., 2024, "A Fully 3D-Printed Flexible Polymeric Heat Pipe," ASME Journal of Thermal Science and Engineering Applications, 16(9), p. 091009.

with an inlet water temperature of 22°C

List of Figures

1	PEBB half-substrate with heat-generating components labeled. Image courtesy of Virginia Tech Center for Power	
		2
2	Current PEBB transformer, Virginia Tech Center for Power Electronics Systems (CPES) [3,4]	2
3	StarCCM+ thermal model of airflow cooling with boundaries highlighted. The cold plate boundary on the lower core half is not visible.	4
4	Cross-section temperatures for the airflow cooling, combined loads scenario	5
5	Isometric view (top) and cross-section view (bottom) of PEBB transformer with heat pipe, iteration 1	5
6	Transformer coils with ceramic insulation. Second set of coils are hidden.	6
7	Cross-section temperatures (top) and coil surface temperatures (bottom) for heat pipe iteration 1, combined loads scenario	6
8	Magnetic flux for 430 kHz operations of heat pipe iteration 2	7
9	Core magnetic flux field for a given time step from the quarter transformer model	7
10	Heat pipe (HP) heat losses for S-shaped configuration at different PEBB operational frequencies. Left axis shows the	
		7
11	S-shaped 2-bend heat pipe (left) and L-shaped 1-bend heat pipe (right)	7
12	Cross-section temperatures for heat pipe iteration 3, combined loads scenario	8
13	Quarter model of PEBB transformer heat pipe, iteration 3	8
14	Magnetic flux for 430 kHz operations of heat pipe iteration 3	8
15	Heat pipe (HP) heat losses for L-shaped configuration at different PEBB operational frequencies.	8
16	Isometric view (top) and cross-section view (bottom) of PEBB transformer with the final heat pipe iteration	9
17	Cross-section temperatures for heat pipe final iteration, combined loads scenario	9
18	Half-PEBB model with final transformer heat pipe design integrated	.(
19	Transformer cross-section temperatures for the half-PEBB final heat pipe model, combined loads scenario, at steady state with an inlet water temperature of 22°C	
20	Transformer core surface temperatures for the half-PEBB final heat pipe model, combined loads scenario, at steady state	٦.
20	with an inlet water temperature of 22°C	1
21	MOSFET surface temperatures for the half-PEBB model, combined loads scenario, at steady state with an inlet water	. 1
21	temperature of 22°C, top and side views	. 1
List of	Tables Tables	
1	Thermal Conductivities for the PEBB Transformer Thermal Model	4
2	Transformer operations loss scenarios	4
3	Airflow reference scenario maximum temperatures	5
4	Thermal and weight performance summary: heat pipe iteration 1	6
5	Thermal and weight performance summary: heat pipe iteration 2	6
6	Electromagnetic properties for the PEBB transformer/heat pipe magnetic analysis	7
7	Thermal and weight performance summary: heat pipe iteration 3	8
8	Thermal and weight performance summary: heat pipe final iteration	9
9	Magnetic performance summary: heat pipe final iteration	5
10	Final iteration heat flow at 430 kHz AC operations (with adjusted Q_{max} including 30% safety factor and bends)	9
- 11	Thermal and weight performance summary: half-PEBB final heat pipe design	. (